

5G Network on Wings: A Deep Reinforcement Learning Approach to UAV-based Integrated Access and Backhaul

Hongyi Zhang¹, Jingya Li², Zhiqiang Qi², Xingqin Lin², Anders Aronsson²,
Jan Bosch¹, Helena Holmström Olsson³

¹*Chalmers University of Technology, Gothenburg, Sweden.*

²*Ericsson Research, Ericsson.*

³*Malmö University, Malmö, Sweden.*

Fast and reliable wireless communication has become a critical demand in human life. When natural disasters strike, providing ubiquitous connectivity becomes challenging by using traditional wireless networks. In this context, unmanned aerial vehicle (UAV) based aerial networks offer a promising alternative for fast, flexible, and reliable wireless communications in mission-critical (MC) scenarios. Due to the unique characteristics such as mobility, flexible deployment, and rapid reconfiguration, drones can readily change location dynamically to provide on-demand communications to users on the ground in emergency scenarios. As a result, the usage of UAV base stations (UAV-BSs) has been considered as an appropriate approach for providing rapid connection in MC scenarios. In this paper, we study how to control a UAV-BS in both static and dynamic environments. We investigate a situation in which a macro BS is destroyed as a result of a natural disaster and a UAV-BS is deployed using integrated access and backhaul (IAB) technology to provide coverage for users in the disaster area. We present a data collection system, signaling procedures and machine learning applications for this use case. A deep reinforcement learning algorithm is developed to jointly optimize the tilt of the access and backhaul antennas of the UAV-BS as well as its three-dimensional placement. Evaluation results show that the proposed algorithm can autonomously navigate and configure the UAV-BS to satisfactorily serve the MC users on the ground.

Index Terms—Reinforcement Learning, Integrated access and backhaul, IAB, 5G NR, wireless backhaul, UAV-BS

I. INTRODUCTION

NOWADAYS, traditional cellular infrastructure provides fast and reliable connectivity in most use cases. However, when a natural disaster happens, such traditional wireless base stations (BSs) cannot provide flexibility, low latency services, and the capacity to rapidly adapt to the new environment. In this context, further enhancements of the cellular networks are needed to enable seamless connectivity and on-demand coverage for various challenging scenarios and ensure all data can be delivered and received from any place to the mission-critical (MC) users.

Drones and unmanned aerial vehicles (UAVs) have shown to be effective tools for a variety of purposes for end users, enterprises, and governments over the last decade. They continue to demonstrate their worth as propulsion technology, sensor technology, and avionics advance, with their usability enabling newer and more applications in a wide range of sectors. As a result, the global market for commercial drones, urban air traffic, and drone deliveries have continued to expand at a rapid pace.

Specifically, UAVs can be used to carry deployable BSs to provide additional or on-demand coverage to users, especially when providing MC services, thanks to their good mobility and higher chances of light-of-sight (LOS) propagation. However, there are a number of challenges when implementing UAV-BS assisted wireless communication networks in practice [1] [2]. The system performance and user experience are significantly impacted by the deployment and configuration of a UAV-BS, including the UAV's flying altitude, operation time, antenna capabilities, transmit power, etc. While optimizing these parameters to provide on-demand access services, it is also necessary to maintain a good backhaul link between the UAV-BS

and traditional BSs on the ground. The optimization problem becomes even more complicated when considering different system loads and dynamic user distribution. In some cases where multiple UAV-BSs are needed to cover a wide area, the complexity of providing reliable and scalable backhaul links between different UAV-BSs will further increase.

A. Related Work

In recent years, UAV-BS assisted wireless communication networks have attracted significant attention from both industry and academia [3]–[7]. To guarantee a robust wireless connection between the UAV-BSs and the core network, more and more research work has started working on improving the wireless backhaul link [8]–[12]. Authors in [8] assume that all the UAV-BSs are flying at a fixed height, and a robust backbone network among UAV-BSs is guaranteed by ensuring that there is always at least one path between any UAV-BS and a BS on the ground if one UAV-BS fails. Then they investigate the rapid UAV deployment problem by minimizing the number of UAVs to provide on-demand coverage for as many users as possible. In [9], optimal 3-D deployment of a UAV-BS is investigated to maximize the number of connected users with different service requirements by considering the limitation of wireless backhaul links. In [10], the limitation of backhaul and access capacities is also considered, and a heuristic algorithm is proposed to optimize the UAV navigation and bandwidth allocation. Similar to [9], the authors in [12] also investigate a coverage improvement problem enabled by UAV-BS with backhaul limitation but with a machine learning (ML) based solution.

Enabled by 5G new radio (NR), the integrated access and backhaul (IAB) feature can be applied to wirelessly integrate

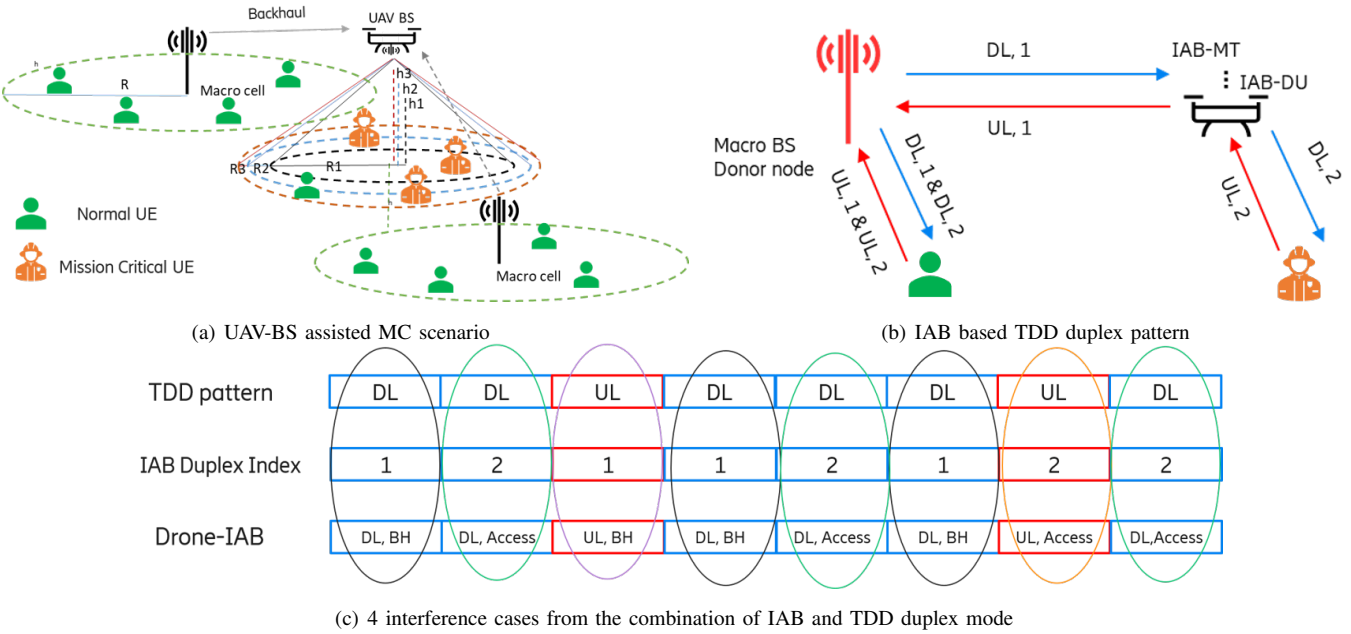


Fig. 1: A UAV-BS assisted wireless network design enabled by a half duplex IAB operation

multiple UAV-BSs to an existing cellular network seamlessly [13]. Figure 1 shows an example of UAV-BS assisted network deployment using IAB technology. The macro-BSs who have connections with the core network are serving the normal users, and some of them can also be acting as donor-BSs, who can provide wireless backhaul connection to the flying UAV-BS. Based on the wireless backhaul link, the UAV-BS is acting as an IAB node, which can be deployed at different locations to provide on-demand services to MC users and/or normal users who are out of the coverage of the existing mobile network. To evaluate the performance of the UAV-assisted wireless system enabled by IAB, authors in [11] propose a dedicated dynamic algorithm based on the particle swarm optimization (PSO) method to optimize the throughput and user fairness. By intertwining different spatial configurations of the UAVs with the spatial distribution of ground users, [14] proposes an interference management algorithm to jointly optimize the access and backhaul transmissions. Their results prove that both coverage and capacity can be improved.

Due to the characteristics of revealing implicit features in large amounts of data, the ML methodology draws growing attention and has been extensively applied in various fields. As a sub-field of ML, agent-based reinforcement learning (RL) features in interacting with the external environment and providing optimized action strategy. Hence, it has been used to solve complicated optimization problems that are difficult to be addressed by traditional methods. As two of the promising technologies for the next-generation wireless communication networks, it is natural to combine ML with deployable UAV-BS to solve high complexity optimization problems [15], [16].

Specifically, ML is frequently used to solve problems on deployment [12], [17], [18], scheduling [19]–[22], trajectory [23]–[26] and navigation [27]–[30] in UAV assisted network. In [17], a deep RL-based method is proposed for UAV control to improve coverage, fairness, and energy efficiency in a multi-UAV scenario. To solve the scheduling problem in a

high mobility environment, the authors in [19] develop a dynamic time-division duplex (TDD) configuration method to perform intelligent scheduling. Based on the experience replay mechanism of deep Q-learning, the proposed algorithm can adaptively adjust the TDD configuration, and improve the throughput and packet loss rate. From the perspective of distributed learning, [20] proposes a framework based on asynchronous federated learning in a multi-UAV network, which enables local training without transmitting a significant amount of data to a central server. In this framework, an asynchronous algorithm is introduced to jointly optimize UAV deployment and scheduling with enhanced learning efficiency.

For ML-based trajectory and navigation, the authors in [23] investigate a trajectory strategy for a UAV-BS by formulating the uplink rate optimization problem as a Markov decision process without user-side information. To enable UAV autonomous navigation in large-scale complex environments, an online deep RL-based method is proposed in [27] by mapping UAV's measurement into control signals. Furthermore, to guarantee that the UAV always navigates towards the optimal direction, authors in [28] enhance the deep RL algorithm by introducing a sparse reward scheme and the proposed method outperforms some existing algorithms.

Additionally, the limited battery life of a UAV restricts its flying time, which in turn affects the service availability that can be provided by the UAV. Therefore, many works have been focusing on designing energy-efficient UAV deployment or configuration schemes either with non-ML [3], [31], [32] or ML methodologies [26], [33], [34].

B. Contributions

In this paper, we consider an MC scenario, where a UAV-BS assisted network is set up for providing temporary on-demand coverage to MC users in a disaster area. Compared with the related works, we propose in this paper a novel RL algorithm to autonomously configure and control a UAV-BS. The UAV-BS is integrated into the existing cellular network using IAB.

The algorithm jointly optimizes the antenna configuration and the 3-D location of the UAV-BS to best serve MC users on the ground while maintaining a good backhaul connection between the UAV-BS and the BSs on the ground. Moreover, a framework and the corresponding signaling procedures are proposed from the perspective of implementation. Last but not least, the designed RL-based algorithm shows remarkable performance in both static and dynamic environments, while the efficiency of the proposed algorithm is also validated.

In our previous paper [35], we presented and validated a deep Q-network (DQN)-based UAV-BS control algorithm on an empirical use case. In this paper, we have further extended our previous work to include the following new findings:

- 1) Different alternatives of framework and signaling procedures are proposed to support applying centralized or distributed ML for the considered use case in an IAB network architecture.
- 2) Rather than employing a single static set for algorithm training and validation, a dynamic environment is used by incorporating MC user mobility. The validation set has grown to include nine distinct phases.
- 3) We introduce two novel strategies, i.e., adaptive exploration control and value-based action selection for the RL algorithm so that the algorithm itself can adapt to a dynamic environment (e.g., MC user movement, traffic load changes) in a fast and efficient way.
- 4) We validate the proposed RL algorithm in a continuously changing environment with nine consecutive MC user movement phases. Our results show that the proposed algorithm can create a generalized model and assist in updating the decision making on UAV-BS configuration and navigation in a dynamic environment.

The remainder of this paper is structured as follows. Section II introduces the use case and system model considered in this paper. In section III, we propose a framework and signalling procedures to enable ML in an IAB network architecture. Section IV discusses our proposed ML algorithm. Section V presents the system-level simulation results and evaluates the proposed RL algorithm. In Section VI, we summarize our findings and discuss the future work.

II. SYSTEM MODEL AND PROBLEM FORMULATION

A. System Model

For the system model, we consider a multi-cell mobile cellular network, consisting of a public network and a deployable network, as shown in Figure 2. Initially, there were seven macro-BSs serving users uniformly distributed in the whole area. However, one of the macro-BSs in the center of the scenario is damaged due to, e.g., a natural disaster that creates a coverage hole. For users in the central emergency area with a predefined 350 m radius, they might have very limited or no connectivity with the public network. Hence, a UAV-BS, which is integrated into the public network using IAB technology, is set up to provide temporary or additional coverage to the MC users located in this emergency area. In the considered scenario, there are two types of users: MC users and normal users. The users located in the MC area are marked as MC

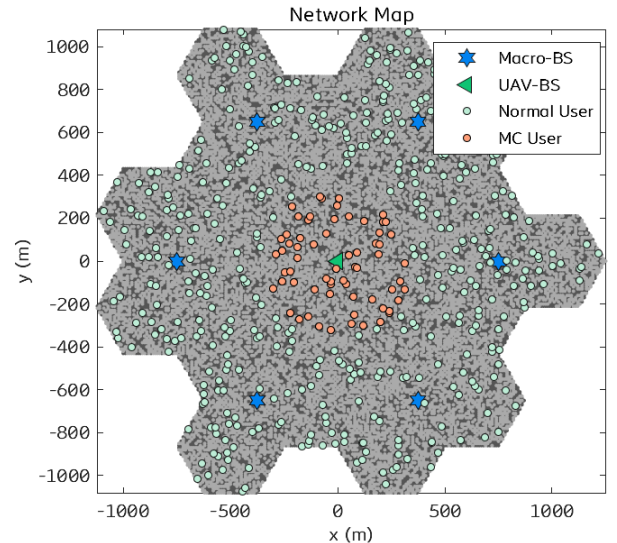


Fig. 2: System model: a UAV-BS assisted network deployment

users, while the others are normal users. A user equipment (UE), either an MC user or a normal user, can select either a macro-BS or the UAV-BS as its serving BS, based on the wireless link qualities between the UE and these BSs.

For the public network in this paper, we use a rural-macro propagation model, which is reused for UAV-BS because the UAV-BS in the current scenario is deployed lower than 35 m [36]. For the traffic pattern design, we apply a dynamic traffic model. All the users are randomly dropped in the scenario. For each time slot, the users are activated with a predefined arriving rate. Only these activated users can be scheduled and initiate fixed-size data transmission based on the link quality (both access and backhaul links) and system load for downlink and uplink, respectively. When the data transmission is completed, the user will leave the system and wait to be activated again. Then the user throughput can be calculated with actually served traffic and consumed time to deliver the traffic. To better reflect the impact of UAV-BS configuration in case of different load situations, two types of load modes are designed with different user arriving rates: heavy load and light load.

B. IAB Configuration

As mentioned before, the UAV-BS works as an IAB node in the current scenario. It will measure the wireless link to the six macro-BSs and select one with the best link quality as its donor-BS. Once the wireless backhaul link between the UAV-BS and its donor-BS is established, the three sectors of the UAV-BS will share this wireless backhaul link and provide access service to both normal users and MC users. For the users served by the UAV-BS, the corresponding throughput depends not only on the access link but also on the wireless backhaul link.

While selecting the access links, the users with too bad link quality, for instance, below a certain threshold, will be dropped. Then each non-dropped user can select its serving BS (a macro-BS or a UAV-BS) based on the end-to-end wireless

path quality, which includes both the backhaul and access links if the UAV-BS is selected as the serving BS.

To reduce the complexity and the load-bearing of the UAV-BS, it is assumed that the same antenna configuration is applied for both access and backhaul antennas of the UAV-BS.

In the current system, the TDD operation is applied, and the time slot pattern consists of downlink (DL), DL, uplink (UL), and DL, which is repeated with a periodicity of 2 ms. Considering that the 100 MHz bandwidth is shared between backhaul and access links, different time slots should be reserved for both links, which is denoted by the IAB duplex index as shown in Figure 1(c). Hence, two full TDD periods are required to cover all the cases, which lead to a total of eight combinations and four interference cases, denoted as: DL1, DL2, UL1, and UL2. For the UAV-IAB node, DL1 and UL1 are reserved for backhaul link transmission, while DL2 and UL2 are reserved for providing access services for users. For the donor-BS and all other macro-BSs, all the time slots can be used for access link transmission.

C. Problem Statement

In a multi-network scenario consisting of both existing BSs on the ground and temporarily deployed UAV-BS, the deployment and configuration of the UAV-BS play a critical role in guaranteeing the performance of the target users/services (e.g., MC users/services). It can also impact the overall system performance. As the UAV-BS is connected to the core network using wireless backhaul, it is important to ensure good quality of both the backhaul and access links when performing this system optimization. In addition, the limitations on UAV's flying altitude, antenna capabilities, and other key parameters also put additional constraints on the optimization problem. Furthermore, the optimal solution depends on many factors like network traffic load distribution, quality of service (QoS) requirements, user movements, transmit power, and antenna settings at the BSs on the ground. Therefore, jointly optimizing these parameters of UAV-BS is a complex system-level optimization problem that needs to be solved in a dynamic changing environment.

In order to best serve target users while also maintaining a good backhaul link quality between UAV-BS and its donor-BS, we aim to solve the following research problems: 1) Design an RL algorithm to jointly optimize the backhaul, access antenna, and the 3-D location configurations of the UAV-BS. 2) Find a UAV-BS movement strategy to accommodate the dynamically changing user distribution.

III. FUNCTIONAL FRAMEWORK AND SIGNALING PROCEDURE FOR ML

In this section, we introduce a functional framework for enabling an intelligent radio access network (RAN). We also propose several signaling procedures based on this functional framework to apply ML to the considered use case described in the previous section.

A. Functional Framework for RAN Intelligence

To provide guidance on designing intelligent RAN enabled by ML, the 3rd Generation Partnership Project (3GPP) initiated a study on enhancement for data collection for 5G NR in Release 17 [37], where high-level principles and corresponding functional framework for RAN intelligence are introduced. This functional framework consists of different ML functionalities, including Data Collection, Model Training, Model Inference, and Actor. Based on this functional framework, we define each ML functionality for our considered use case as follows.

The Data Collection function is responsible for collecting input data (e.g., measurements and performance metrics from interested users and the related BSs) for ML. The collected data is divided into two sub-sets as training data and inference data. They are provided to the Model Training and Model Inference functions, respectively. The Data Collection function may also receive feedback from other learning functions and adjust its configuration (e.g., data collection periodicity and collected data type) accordingly.

The Model Training function performs the ML model training, validation, and testing of the ML model using the training data. Then, it sends the ML model to the Model Inference function.

The Model Inference function provides the learning outcome using the ML model received from the Model Training function and the inference data delivered from the Data Collection function.

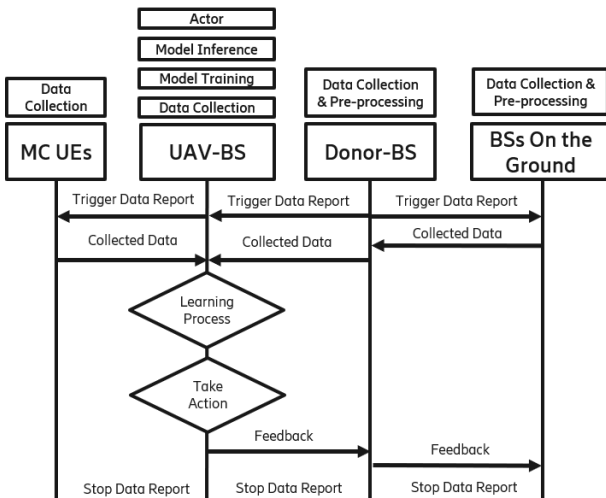
The Actor function receives the output from the Model Inference function and triggers or performs corresponding actions, e.g., adjusting antenna configuration and navigating the UAV-BS to a new position in the considered use case.

B. Intelligence-Based Signaling Procedure

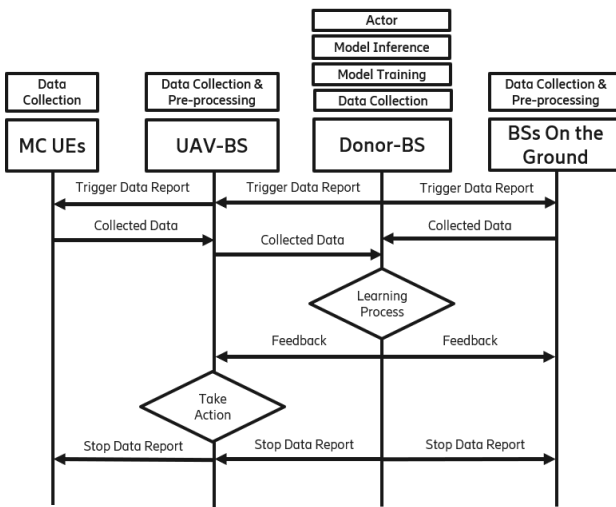
In this subsection, we present three different signaling procedures to illustrate how the proposed functional framework can be utilized to support applying centralized or distributed ML for the considered use case, i.e., jointly optimizing the antenna configuration and the 3-D location of a UAV-BS in an IAB network architecture. Depending on where the ML model is hosted and how the ML algorithm is executed (distributed or centralized), three major scenarios are introduced in the following subsections. Here, we consider a single-hop IAB operation. The UAV-BS is connected to its donor-BS via a direct single-hop wireless backhaul link, and it provides wireless access links to connected users. In addition, we assume that the data collection for ML is triggered by the donor-BS. The proposed signaling procedures can also be extended to other cases like multi-hop IAB operations and UAV-BS triggered data collection.

1) Case 1: UAV-BS Hosting ML Model

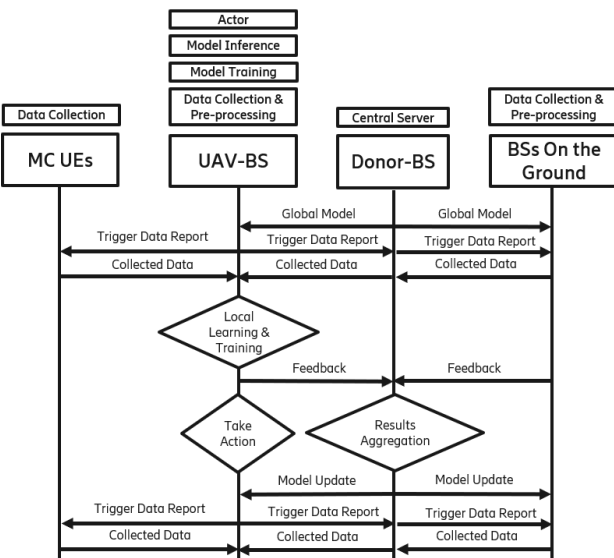
For Case 1, as shown in Figure 3(a), the UAV-BS is connected to a donor-BS via single-hop wireless backhauling, and it will provide wireless access links to MC UEs within its coverage. Data collection for optimizing the UAV-BS's configuration and deployment is triggered by a donor-BS, while the collected data can be raw data based on the measurements,



(a) Case 1: UAV-BS Hosting ML Model



(b) Case 2: Donor-BS Hosting ML Model



(c) Case 3: UAV-BS Hosting ML Model & Donor-BS as Central Server

Fig. 3: Signaling procedures to support applying ML for the considered use case

key performance indicators (KPIs), or post-processed data. The ML related functions, including Data Collection, Model Training, Model Inference, and Actor, are all hosted in the UAV-BS, which reduces the signaling overhead and latency caused by ML-related information exchange between the UAV-BS and the other network entities. If multiple UAV-BSs are used in the considered single-hop IAB operation scenario, the proposed singling procedure in Case 1 allows each UAV-BS to make its local decision independently. Hence, this signaling procedure can be used to support distributed ML, and it consists of the following key steps:

- 1): Data requests triggered by a donor-BS: After a UAV-BS completes its network integration procedure, or when a UAV-BS mobility event has been detected (e.g., a UAV-BS has adjusted its location), the donor-BS triggers data collection to assist the UAV-BS in optimizing its configuration and deployment by sending a data request message to the relevant users and BSs.
- 2): Data collection at the UAV-BS: After receiving the data request, MC users, the donor-BS, and related BSs on the ground will send the requested data to the UAV-BS. The collected data can include: a) data collected by the UAV-BS itself, e.g., from its connected MC users, radio measurements, and onboard sensors; b) data firstly reported from a set of users and a set of BSs on the ground, and then forwarded to the UAV-BS.
- 3): Learning process in the UAV-BS: After processing the collected data, the Model Training and Model Inference functions at the UAV-BS are initiated accordingly. When the model training procedure is finished, a set of ML-related parameters are generated corresponding to the trained model. Then, the Model Inference function will develop the suggested deployment strategy and configuration based on the trained model and collected inference data.
- 4): The UAV-BS takes action: Based on the output of the Model Inference, the Actor function in the UAV-BS performs antenna tilt, location adjustment, and other suggested configurations.
- 5): The UAV-BS sends feedback to its donor-BS, who can then forward the feedback or action recommendations to the other related BSs.
- 6): With the feedback from the UAV-BS as input data, the donor-BS and/or the related BSs adjust their configuration (e.g., antenna tilt, transmit power, etc.). Finally, the donor-BS stops requesting data.

In the above procedure, steps 2)-6) can repeat till certain criteria are fulfilled (e.g., the ML algorithm can steadily provide optimized output). The donor-BS can then stop the learning process by sending a stop data reporting message to its connected users and the other related BSs.

2) Case 2: Donor-BS Hosting ML Model

For Case 2, as shown in Figure 3(b), the major difference from Case 1 is that all ML-related functions are hosted at the donor-BS. This can relax the hardware requirements and reduce the computational complexity for the UAV-BS, which can in turn reduce the power consumption and increase the

flying time of the UAV-BS. The signaling procedure can be used to support centralized ML algorithms and it consists of the following key steps:

- 1)-3): Similar to Case 1, except that the data collection and learning process are performed at the donor-BS.
- 4): The donor-BS sends feedback to the UAV-BSs and other related BSs. The feedback includes recommendations on the configuration/adjustment of these BSs.
- 5): The UAV-BS takes action: The UAV-BS performs (re)configuration and/or movement based on the feedback from the Actor function in its donor-BS.
- 6): With the feedback from the donor-BS as input data, the related BSs adjust their configuration (e.g., antenna tilt, transmit power). Finally, the donor-BS stops requesting data.

Similar to case 1, step 2)-6) in Case 2 can also repeat till certain criteria are fulfilled (e.g., the ML algorithm can steadily provide optimized output).

3) Case 3: UAV-BS Hosting ML Model & Donor-BS as Central Server

For Case 3, as shown in Figure 3(c), a signaling procedure is proposed to support hybrid ML algorithms, where a centralized ML model is maintained at a central service (i.e., the donor-BS in our case) and a local copy of the ML model is distributed to each UAV-BS. The donor-BS aggregates the training results received from the UAV-BSs and updates its central ML model. After the UAV-BS finishes its model training, a refined local ML model will be generated and feedback to the donor. The signaling procedure consists of the following key steps:

- 1): Model update triggered by a donor-BS: After a UAV-BS completes its network integration procedure, or when a UAV-BS mobility event has been detected (e.g., a UAV-BS has adjusted its location), the donor-BS triggers the central ML model updates by sending a copy of the centralized ML model to the UAV-BS.

- 2): Data collection at the UAV-BS: After receiving the global learning model, the UAV-BS triggers data collection to optimize its configuration and deployment by sending a data request message to the relevant users and its donor-BS. The collected data can be the same as the candidate parameters in Case 1.
- 3): Learning process in the UAV-BS: Each UAV BS can gradually learn and update the received global model based on its locally collected data. When the model update is finished, a refined local model is generated and will be sent back to its donor-BS.
- 4): The UAV-BS takes action: Based on the output of the local ML Model Inference, the Actor function in the UAV-BS performs antenna tilt, location adjustment, and other suggested configurations.
- 5): The UAV-BS sends feedback to the central server (donor-BS). The feedback includes training results (e.g., trained local model) from the UAV-BS.
- 6): Based on the feedback from the UAV-BS, the donor-BS aggregates the training results (e.g., trained local model) transferred from all related UAV BSs, and updates the centralized ML model.
- 7): Repeat the above process if needed.

IV. ML-BASED SOLUTION

A. Modeling of ML Environment

In this section, we describe how we transform and model the considered use case in an ML environment. Three important components, including the state space, action space, and reward function, are constructed in order to design an RL algorithm to jointly optimize the antenna tilt and the 3-D position of a UAV-BS in an IAB network.

1) State Space

In our case, a UAV-BS state at a given time instance t has four dimensions, including the UAV-BS's antenna tilt and its 3-D position.

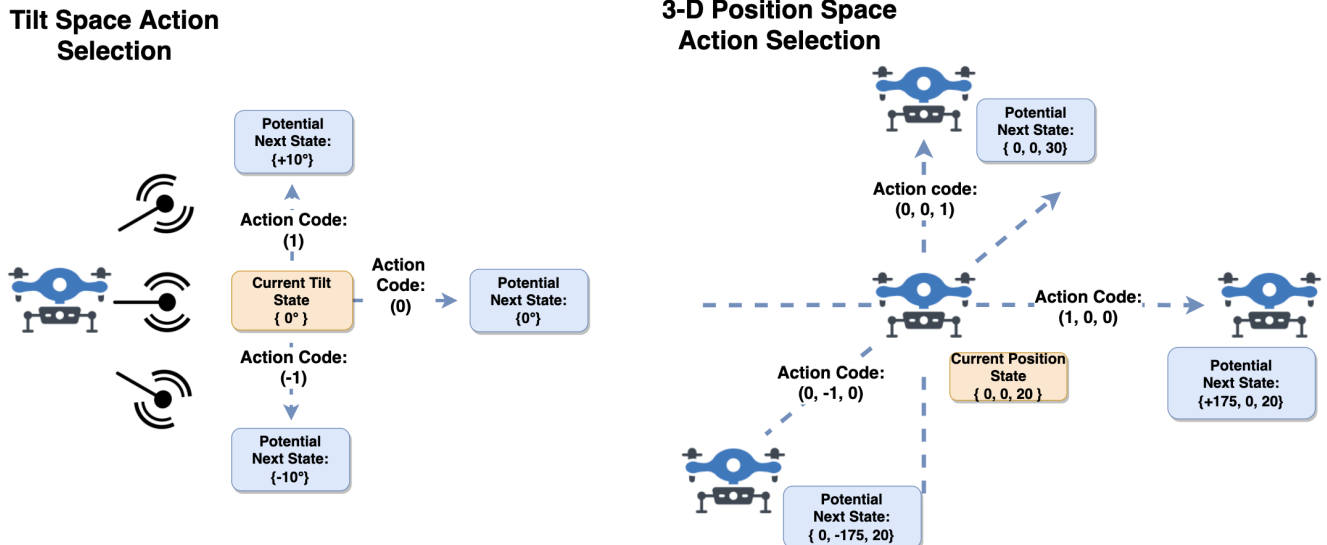


Fig. 4: Example of the state transition from current state $\{0^\circ, 0, 0, 20\}$

We use $\mathcal{T}_t = \{\sigma_t\}$ to represent the electrical tilt value of the access and backhaul antenna and $\mathcal{P}_t = \{x_t, y_t, z_t\}$ to denote the 3-D position of the UAV-BS at time t . Then, a UAV-BS's state at a given time instance t is denoted as $s_t = \{\sigma_t, x_t, y_t, z_t\}$. Table I shows the candidate values of these state dimensions:

TABLE I: Candidate values for each state dimension in the simulation environment

Tilt \mathcal{T} Space	Candidate Values
σ	$[-30, -20, -10, 0, +10, +20, +30]$ degree
3-D position \mathcal{P} Space	Candidate Values
x	$[-350, -175, 0, +175, +350]$ meters
y	$[-350, -175, 0, +175, +350]$ meters
z	$[10, 20, 30, 35]$ meters

The candidate values of 3-D space location x , y and z axis cover the disaster area shown in Figure 2. For the candidate antenna tilt values, a positive tilt value means applying an electrical down-tilt to the access and backhaul antenna, and a negative tilt value maps to applying an electrical up-tilt to the antenna.

2) Action Space

In order to enable UAV-BS to control its state, for each state dimension, we defined three potential action options and the UAV-BS chooses an action from three candidate options. These three alternative action options are denoted by the three digits: $-1, 0, 1$, where “ -1 ” indicates that the UAV-BS decreases the status value at this state dimension by one step from its current value; “ 0 ” indicates that the UAV-BS does not need to take any action at this state dimension and keeps its current value; “ 1 ” indicates that the UAV-BS increases the status value at this state dimension by one step from its current value.

For example, if the tilt value of the UAV-BS (i.e. the value of the σ dimension) equals 0 degree, an action coded by “ -1 ” for this dimension means that the UAV-BS will select an action to reduce the tilt value to -10 degree, an action coded by “ 0 ” implies that the UAV-BS will hold the current tilt value (0 degree), and an action coded by “ 1 ” implies that the UAV-BS will increase the tilt value to $+10$ degree. The same policy is applied to all dimensions of the state space.

Since there are three action alternatives for each space state, the action pool for tilt space can then be programmed to a action list $\mathcal{T} = [(-1), (0), (1)]$ while for 3-D position space, the pool has 27 action candidates that may be programmed to a action list $\mathcal{P} = [(-1, -1, -1), (-1, -1, 0), (-1, -1, 1), (-1, 0, -1), (1, 1, -1), (1, 1, 0), (1, 1, 1)]$. As a result, if we combine the action of tilt space and 3-D position space, at any given moment t , the UAV-BS can thus choose an action a_t from these 81 alternatives. Figure 4 depicts a state transition from the specified state $s_t = \{0^\circ, 0, 0, 20\}$.

3) Reward Function Design

It is more critical to serve as many MC users as possible with appropriate service quality than to maximize the peak rate of a subset of MC users. As a result, for the RL algorithm's reward function design, we pick six essential feature metrics to describe the overall QoS for MC users, including:

- The drop rates of MC users for UL and DL (β_{ul}, β_{dl}), which reflect the percentage of unserved MC users.
- The 50% throughput values of MC users for both UL and DL ($\alpha_{ul-50\%}, \alpha_{dl-50\%}$), which represent the average performance of the MC users, and
- The 5% throughput values of MC users for both UL and DL ($\alpha_{ul-5\%}, \alpha_{dl-5\%}$), which represent the “worst” performance of the MC users.

The reward function is built as a weighted sum of these six feature values to balance these critical performance indicators, as shown below. Before the model, all characteristics are normalised using min-max normalization, thus the values are constrained within the range $[0, 1]$.

$$R_s = \omega_1 \times \frac{(1 - \beta_{dl}) + (1 - \beta_{ul})}{2} + \omega_2 \times \frac{(\alpha_{ul-5\%} + \alpha_{dl-5\%})}{2} + \omega_3 \times \frac{(\alpha_{ul-50\%} + \alpha_{dl-50\%})}{2} \quad (1)$$

Furthermore, we set $\omega_1 + \omega_2 + \omega_3 = 1$ to normalize the reward value such that R_s is between $[0, 1]$. To emphasize the significance of supporting all MC users, we assign higher weights to user drop rates and 5% MC-user throughput metrics. This is because, in the MC use cases, we must first prioritize that all users have access to the communication service rather than focusing on optimizing the communication quality of a small subset. In this paper, our method uses the weight values $\omega_1 = 0.5$, $\omega_2 = 0.3$ and $\omega_3 = 0.2$.

B. RL Algorithm Design

In this section, we design an RL algorithm to solve the optimization problem of the considered use case. RL is distinct from supervised and unsupervised learning in the field of ML in that supervised learning is performed from a training set with annotations provided by an external supervisor (task-driven), whereas unsupervised learning is typically a process of discovering the implicit structure in unannotated data (data-driven). RL is suitable for this case since the method provides a unique feature: the trade-off between exploration and exploitation, in which an intelligence agent must benefit from prior experience while still subjecting itself to trial and error, allowing for a larger action selection space in the future (i.e., learning from mistakes).

In order to achieve better self-control decisions for our scenario, we applied deep Q-network (DQN) as our base RL algorithm. The algorithm was firstly proposed by Mnih et al. in [38] [39] by combining convolutional neural networks with Q-learning algorithms [40] in traditional RL. The approach has been frequently used in gaming and static environments. However, the original approach is incapable of adapting to our MC situation due to environmental changes. To address these issues, we have proposed two significant improvements in our autonomous UAV-BS control algorithm (Algorithm 1): adaptive exploration control and value-based action selection.

1) Adaptive Exploration (AE)

Because of the environmental changes, the original DQN model needs to be updated to accommodate feature value

Algorithm 1: Deep Reinforcement Learning with adaptive exploration and value-based action selection

```

Initialize the agent's replay memory Buffer  $\mathcal{D}$  to
capacity  $N$ 
Initialize action-value function  $Q$  with two random sets
of weights  $\theta, \theta'$ 
Initialize exploration probability  $\varepsilon$  to 1
Set previous reward value  $r_p$  to 0
for Iteration = 1,  $M$  do
  for  $t = 1, T$  do
     $\mathcal{T}_t, \mathcal{P}_t \leftarrow \text{Action\_Selection}(r_p, r_t, \varepsilon)$ 
     $a_t = \{\mathcal{T}_t, \mathcal{P}_t\}$ 
    Set  $r_p = r_t$ 
    Decode  $a_t$  to action options in four state
    dimensions and execute the actions
    Collect reward  $r_t$  and observe the agent's next state
     $\mathcal{T}_{t+1} \leftarrow \{\sigma_{t+1}\}, \mathcal{P}_{t+1} \leftarrow \{x_{t+1}, y_{t+1}, z_{t+1}\}$ 
    Set  $s_{t+1} = \{\mathcal{T}_{t+1}, \mathcal{P}_{t+1}\}$ 
    Store the state transition  $(s_t, a_t, r_t, s_{t+1})$  in  $\mathcal{D}$ 
     $\mathcal{A}_s, \mathcal{A}_o \leftarrow \text{Action\_Grouping}(a_t)$ 
    Sample mini-batch of transitions  $(s_j, a_j, r_j, s_{j+1})$ 
    from buffer  $\mathcal{D}$ 
    if  $s_{j+1}$  is terminal then
      Set  $y_j = r_j$ 
    else
      Set  $y_j = r_j + \gamma \max_{a'} Q(s_{j+1}, a'; \theta')$ 
    end if
    Perform a gradient descent step using targets  $y_j$ 
    with respect to the online parameters  $\theta$ 
    Set  $\theta' \leftarrow \theta$ 
     $\varepsilon \leftarrow \text{Adaptive\_Exploration}(r_p, r_t, \varepsilon)$ 
  end for
end for

```

changes. As a result, we create a dynamic exploration probability triggered by a substantial decline in reward value. Following the completion of each learning iteration, the final reward value is checked and compared to the pre-defined reward-drop and upper reward thresholds. Based on the outcome, the exploration probability ε will be adjusted.

The UAV-BS initially explores the state space and then performs Q-value iterations at each training episode. When deciding whether to take an action that gives the maximum reward value or randomly explore a new state, a ε -greedy exploration is used. The parameter ε determines the likelihood of exploration. Each training step's data is saved in a replay batch \mathcal{D} . Each row of \mathcal{D} holds the tuple (s_t, a_t, r_t, s_{t+1}) , which represents the current state, action, reward, and next state for a training step. Samples will be chosen at random and used to update the Q value model.

The most recent reward value is reviewed and compared to a pre-defined reward-drop threshold and an upper reward threshold. Then, the exploration probability is updated by checking the following three conditions: (Algorithm 2):

- If the most recent reward value is less than the prior reward, and the difference is greater than the reward drop threshold, the exploration probability is increased to 0.1.
- If the most recent reward value exceeds the higher reward

threshold, we can conclude that the algorithm has already located the optimal zone capable of delivering a reliable connection to MC users. The likelihood of exploration will be matched to the probability of completion.

- Otherwise, the exploration probability will multiply by an exploration decay and fall linearly after each learning cycle.

Algorithm 2: Adaptive Exploration Algorithm (AE)

```

Set restarting exploration probability  $\varepsilon_{Restart}$ 
to 0.1
Set ending exploration probability  $\varepsilon_{End}$  to 0.0001
Set exploration decay  $\varrho$  to 0.995
Function Adaptive_Exploration( $r_p, r_t, \varepsilon$ ):
  if  $r_p - r_t >$  Drop threshold then
    Set  $\varepsilon = \varepsilon_{Restart}$ 
  else if  $r_t >$  Upper reward threshold then
    Set  $\varepsilon = \varepsilon_{End}$ 
  else
    Set  $\varepsilon = \varepsilon \times \varrho$ 
  end if
  return  $\varepsilon$ 

```

Algorithm 3: Value-based action selection (VAS)

```

Set grouping threshold  $\beta$  to 0
Function Action_Grouping( $a_t$ ):
   $\mathcal{P}_t \leftarrow a_t = \mathcal{T}_t, \mathcal{P}_t$ 
  for all potential next action  $\mathcal{P}_{t+1}$  do
    if  $\vec{\mathcal{P}}_t \cdot \vec{\mathcal{P}}_{t+1} > \beta$  then
      Append  $\vec{\mathcal{P}}_{t+1}$  to  $\mathcal{A}_s$ 
    else
      Append  $\vec{\mathcal{P}}_{t+1}$  to  $\mathcal{A}_o$ 
    end if
  end for
  return  $\mathcal{A}_s, \mathcal{A}_o$ 

Function Action_Selection( $r_p, r_t, \varepsilon$ ):
  if  $r_t \geq r_p$  then
    Select a random action  $\mathcal{P}_t$  with probability  $\varepsilon$ 
    from the same consequence 3-D position
    action pool  $\mathcal{A}_s$ 
    Randomly select a tilt space action  $\mathcal{T}_t$ 
  else
    Select a random action  $\mathcal{P}_t$  with probability  $\varepsilon$ 
    from the opposite consequence 3-D position
    action pool  $\mathcal{A}_o$ 
    Randomly select a tilt space action  $\mathcal{T}_t$ 
  end if
  Otherwise, select  $a_t = \arg \max_a Q(s_t, a; \theta)$ 
  return  $\mathcal{T}_t, \mathcal{P}_t$ 

```

2) *Value-Based Action Selection (VAS)*

Although the ε -greedy algorithm can strike a reasonable balance between exploration and exploitation, in some cases the approach utilized for exploration is redundant and time-consuming. The algorithm will choose actions at random

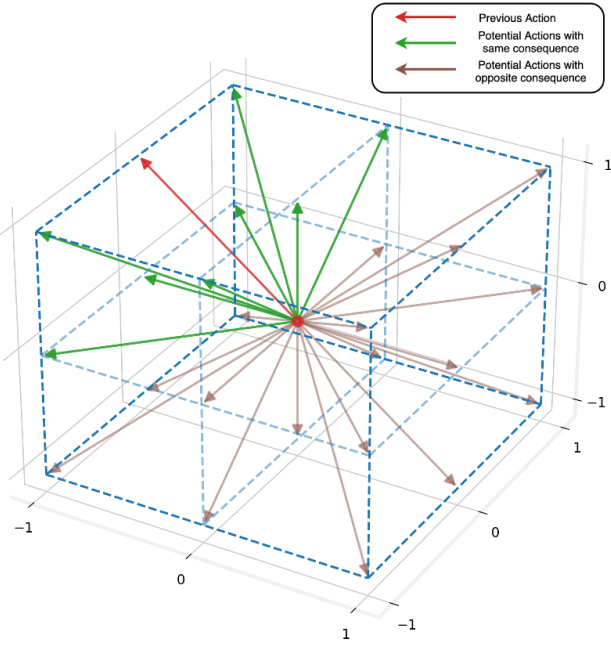


Fig. 5: Diagram of potential set of next actions with same or opposite consequence

throughout the searching stage, which may lengthen the search time. However, when dealing with a large action and state space, random action selection is clearly not an effective strategy and may cause decision-making to be delayed, which is unacceptable in most time-critical businesses. Therefore, we propose a novel value-based action selection strategy (Algorithm 3) which can lead to fast decision making for the UAV-BS when determining its 3-D space location.

As described in the previous section, an agent's 3-D position state at a given time instance t is denoted as $\mathcal{P}_t = \{x_t, y_t, z_t\}$. Since each position state has three dimensions and each state dimension has three action options, the action pool contains in total 27 action candidates that can be programmed to a list of action space $[(-1, -1, -1), (-1, -1, 0), (-1, -1, 1), \dots, (1, 1, 1)]$. Each element in this list can then be regarded as an action vector.

Figure 5 depicts a probable set of next actions with the same or opposite consequence. The consequence is defined as the reward value (or monitored performance metrics) change after an action has been executed. The algorithm will analyze the outcome of past actions. If the prior action decision has a positive outcome (the reward value increases or monitored performance metrics become better) as defined above, the algorithm will choose actions from a pool of following actions with the same consequence. The dot product between two action vectors determines the result. If the dot product is larger than 0, this action vector can be assumed to have the same outcome as the prior action option.

If the previous action decision results in a negative consequence (the reward value decreases or monitored performance metrics become worse), the algorithm will select actions from the pool consisting of potential next actions with the opposite consequence. The opposite consequence is determined by the dot product of two action vectors that is smaller than or

equal to 0. The actions in this pool will result in an opposite consequence compared with the previous action decision. Assume that the previous action vector is $\vec{\mathcal{P}}_t$ while the next potential action vector is $\vec{\mathcal{P}}_{t+1}$:

$$\begin{cases} \vec{\mathcal{P}}_t \cdot \vec{\mathcal{P}}_{t+1} > 0 & \text{Same consequence as previous} \\ \vec{\mathcal{P}}_t \cdot \vec{\mathcal{P}}_{t+1} \leq 0 & \text{Opposite consequence as previous} \end{cases} \quad (2)$$

In Figure 5, the red vector represents the previous action decision. The green vectors are the actions that may result in the same consequence as the red vector, while the brown vectors may result in the opposite consequence.

During the UAV-BS deployment, the algorithm monitors a set of critical system performance values (the reward value). Based on the current and a set of previous performance values, the algorithm will evaluate the consequences caused by the previous action. The algorithm will thus select the action set which will potentially result in positive consequences.

V. SIMULATION RESULTS AND ANALYSIS

In this section, the simulation configuration and scenario deployment are introduced firstly. Then, we investigate the impact of the antenna configuration and 3-D location of the UAV-BS on the performance of MC users in terms of backhaul link rate, throughput, and drop rate by using system-level simulations. Finally, we present the results of proposed RL algorithms for autonomous UAV-BS navigation and configuration.

A. Simulation Configuration and Set-up

To evaluate the performance of the proposed RL algorithm in solving the formulated problem, we build a scenario by considering the predefined system model, and a simulation is executed with a system-level simulator. With the output of the simulation, the proposed RL algorithm can be applied to build a well-trained model, based on which the optimal UAV-BS position and antenna configuration can be found rapidly.

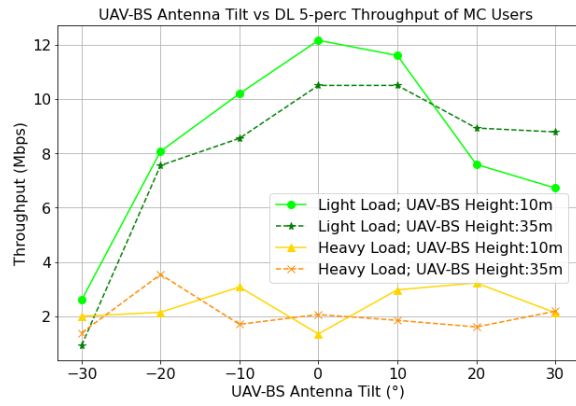
In the simulation, we drop 500 users in the area as shown in Figure 2. The circle area with a 350m radius around the UAV-BS is defined as the MC area. The users located in the MC area are marked as MC users, while the others are normal users. All users follow an arrival model and only arrived users can be considered as activated. To investigate how a well-trained ML model performs in a dynamic environment, we design a set of different user distributions to simulate the case of slow-moving users.

The detailed simulation parameters are shown in Table II.

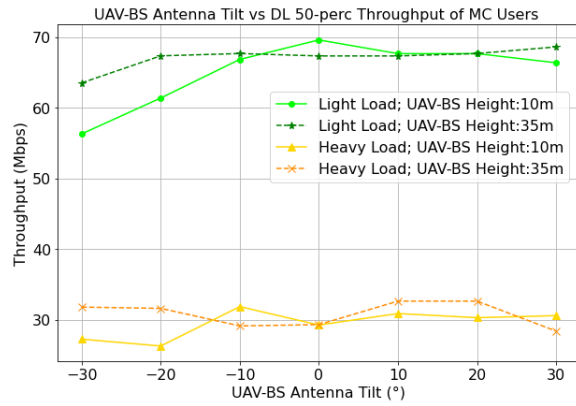
B. System-level Performance Evaluation

Before the ML analysis, we firstly investigate the simulation data from the perspective of a communication system. Figure 6 shows the relationship between UAV-BS antenna tilt and relevant performance metrics including the backhaul link rate of UAV-BS, 5% and 50% throughput of MC users.

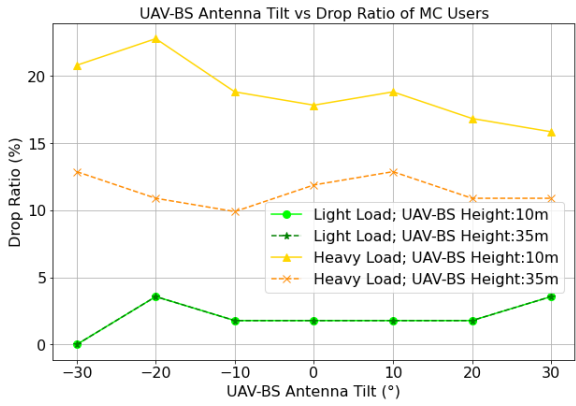
To evaluate the impact of UAV-BS antenna tilt on the performance of MC users, the 2D-position of UAV-BS is fixed



(a) Antenna Tilt vs DL 5% Throughput for MC Users



(b) Antenna Tilt vs DL 50% Throughput for MC Users



(c) Antenna Tilt vs Drop Rate for MC Users

Fig. 6: UAV-BS antenna tilt's impact on MC user throughput (5% and 50%) and MC user drop rate

at the center of the MC area. By comparing Figure 6(a) and Figure 6(b), it can be seen that the impact of antenna tilt on the 5% and 50% throughput of MC users is more visible in the case of light load, while the impact of antenna tilt is negligible in the heavy load case. Specifically, 5% throughput is more sensitive to antenna tilt than 50% throughput. Even though the range change of both metrics in response to antenna tilt is similar, 5% throughput experiences more dramatic changes proportionately. From Figure 6(a) and Figure 6(b), there is no obvious impact of UAV-BS height on both throughput metrics. In Figure 6(c), we can see that both antenna tilt and UAV-BS

TABLE II: Simulation Parameters

Parameter	Value
Carrier Frequency	3.5 GHz
Bandwidth	100 MHz
Duplex Mode	TDD
TDD DL/UL Configuration	DDUD
Inter-Site-Distance (ISD)	750 m
Number of Sectors per Site	3
Radius of MC Area	350 m
Number of MC&Normal Users	500
BS Transmit Power	Macro-BS: 46 dBm; UAV-BS: 40 dBm
UAV-BS Height	10-35 m
User Arriving Rate per Simulation Area	Light load: 270 users/s Heavy load: 540 users/s
Simulation Time	2 s

height have a significant impact on the drop rate of MC users. For the heavy load case, the drop rate is lower in the case of higher UAV-BS height. This is due to a higher chance of LOS propagation if the UAV-BS moves to a higher altitude. For the light load case, it is observed that the curves for two cases with different UAV-BS height overlap, which implies that UAV-BS height has very limited impact in the current context, while the antenna tilt is a dominant factor.

To evaluate the impact of UAV-BS position on the relevant performance metrics, we fix the UAV-BS antenna tilt and height at 0° and 10 m, respectively. Around the MC area, 25 candidate UAV-BS 2D-positions are selected in the form of a 5x5 grid distribution with the position-to-position distance of 175 m, as shown by the centers of 25 circles in Figure 7. Figure 7 gives an overview of the relevant performance metrics in the case of both light and heavy loads while the UAV-BS is deployed in 25 candidate positions. The size of the circles denotes the scaled-down value of the backhaul link rate of UAV-BS, 5% throughput, 50% throughput, and drop rate of MC users. The larger the size is, the higher value for a considered performance metric. For 5% throughput and 50% throughput, the same scaling factor is used; hence, the sizes of circles for these two metrics are comparable. In each sub-figure, the darkness of a circle represents the relative value of the considered performance metric. The darker the color is, the higher value of the performance metric is.

Based on the above assumptions, the optimal UAV-BS position to maximize the backhaul link rate and user throughput can be denoted as the center of the darkest and largest circle in each sub-figure, while for the drop rate we should select the lightest and smallest circle. It can be seen from Figure 7 that the optimal UAV-BS position is different for each performance metric. Even for the same metric, the optimal UAV-BS position is also different for each load case. For backhaul link rate and throughput, it seems the optimal UAV-BS position tends to be near the edge of the MC area, while spontaneously the UAV-BS should stay in the center of the MC area to best serve users. This is because the UAV-BS can keep good backhaul link quality when located near the edge area. When only considering the drop rate, it is easy to understand that the UAV-BS tends to hover in the central area to serve as many users as possible. Hence, optimizing the relevant performance metrics by adjusting UAV-BS position and configuration is a complicated problem, for which ML-based solutions can be

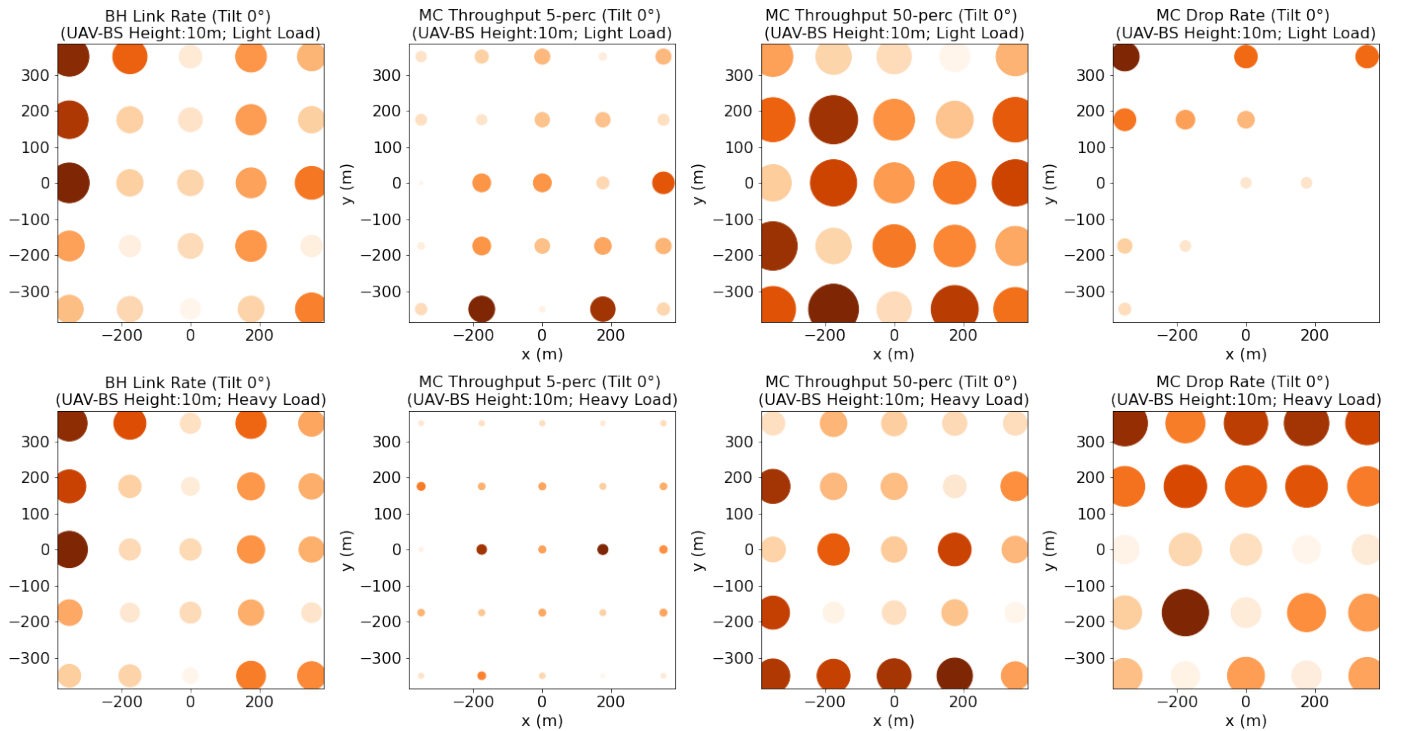


Fig. 7: UAV-BS Position vs Performance for MC Users

applied to find the implicit structure from the collected data.

C. Machine Learning Performance Evaluation

In this section, we present the experimental results of Reinforcement Learning with Adaptive Exploration and Value-based Action Selection (RL-AE&VAS) for autonomously controlling UAV-BS. The result is evaluated using two criteria: (1) six features (specified in Section IV - Modeling of ML Environment) that demonstrate link service quality, and (2) model learning quality in each phase as demonstrated by system reward value. The results are compared to two baseline models: (1) Retrained Reinforcement Learning with VAS (Retrained RL-VAS) in each phase to demonstrate the efficiency of the new algorithm and the importance of using prior knowledge, and (2) baseline Reinforcement Learning (Baseline RL) method, which is a commonly used DQN algorithm without improved mechanisms. As we described before, the experiment contains nine different phases incorporating MC user mobility. When entering a new phase, the algorithms will use the new phase data to learn and update themselves.

The RL-AE&VAS method trains the model from scratch in the training phase and then continuously improves itself in the succeeding validation phases. The previously learnt experience will not be removed for the subsequent sessions. The retrained RL-VAS algorithm removes the past information and randomizes the ML model parameters. When entering a new phase, the algorithm will retrain the model from scratch but with the assistance of an improved mechanism. For the baseline RL algorithm, the algorithm will constantly learn and employ the new data when entering the new phase. However, the algorithm used here is the standard DQN [39], which doesn't have any improved strategy.

For the hyper-parameters of our method, we explored various sets of combinations in order to achieve acceptable results. During the training, the network architecture for a DQN is set to [4 – 16 – 16 – 81], the exploration probability decay is set to 0.995, the learning rate is set to 5×10^{-5} and the number of training iterations at the training phase equals 1000.

We first analyze the algorithm's convergence performance during model training. Figure 8 depicts the reward value as a function of the number of training iterations. Compared to the baseline RL algorithm, we can see that the VAS method can help the UAV-BS quickly discover the near-optimal position and converge at a high-quality level for both light and heavy load conditions. During the validation phase (Phase I - VIII), the proposed algorithm can learn from the past and finally reach the optimal state that provides the highest reward value in both load scenarios using the AE method. Even if the environment has changed and the quality has dropped dramatically, the algorithm can assist the UAV-BS in quickly adjusting and returning to ideal performance.

When we look at the baseline RL approach, the method failed to respond to environmental changes in a short period due to the slow-paced state exploration. When we compared the baseline results to the retrained RL-VAS and RL-AE&VAS, the results showed that our suggested VAS approach can enable UAV-BS quickly converge in most of the validation phases. However, with the retrained RL-VAS, a significant impact may occur on algorithm and service stability if not using previous existing knowledge. When we integrated RL with adaptive exploration and the value-based action selection strategy, the algorithm showed the best performance in terms of convergence speed, the ability to adapt to environmental changes, and stable service quality of our

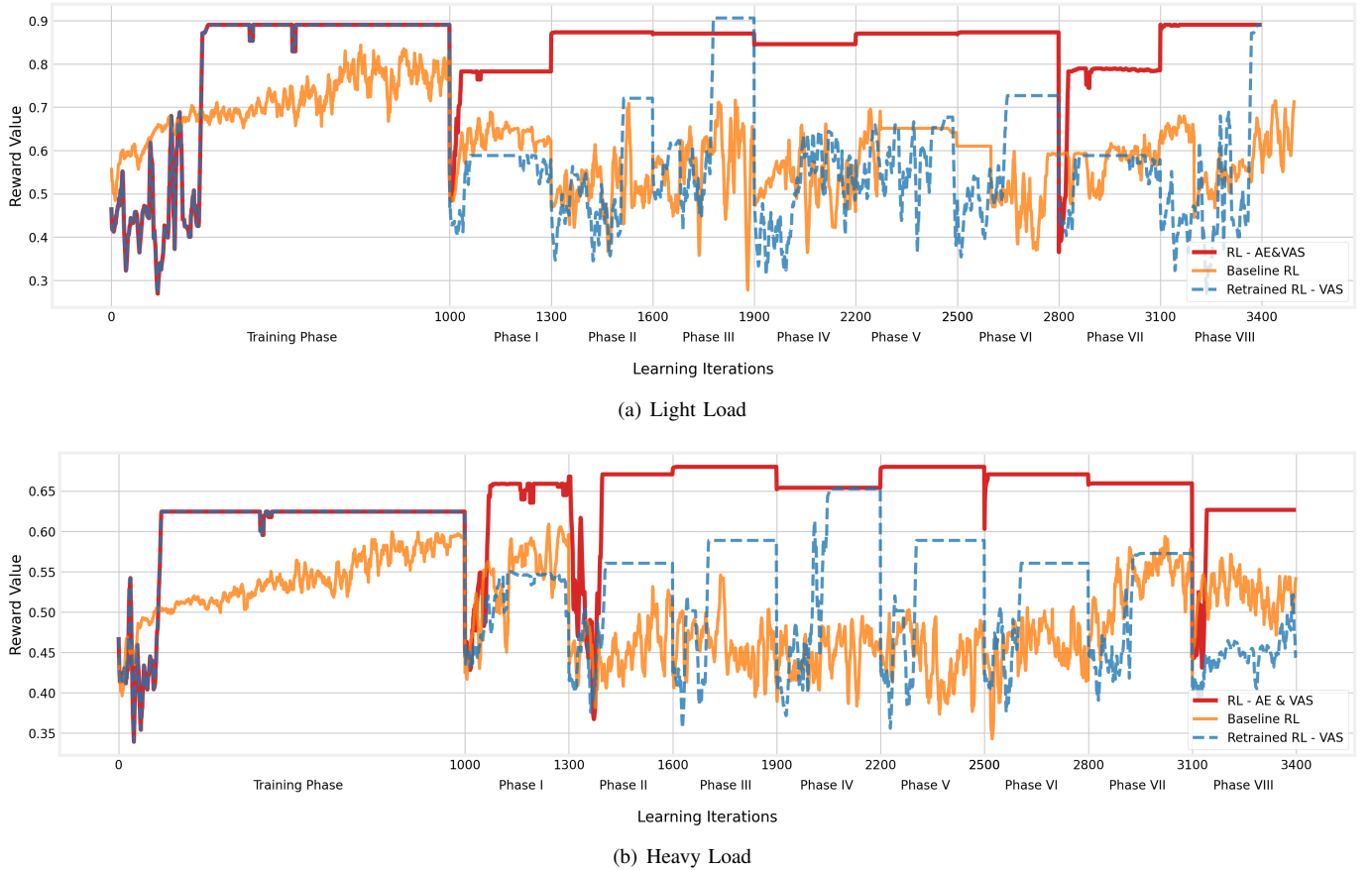


Fig. 8: Reward value with number of learning iterations in two different network traffic load scenarios

suggested RL-AE&VAS method. Comparing the results in the reward value column of Table III leads to the same conclusion.

The average reward value changes during the validation phases are depicted in Figure 9. Because the reward value encompasses all of the essential criteria that must be evaluated during the deployment of the UAV-BS, the value clearly demonstrates the model's quality at each stage. As shown in the figure, our proposed RL-AE&VAS method can assist the UAV-BS in reaching the ideal area, but the baseline model failed to discover a state that can give reliable and satisfactory service to MC users.

More detailed metrics are presented in Table III. The suggested RL-AE&VAS technique gives a reward value (a weighted sum of the six assessed performance measures) of only about 5% to 6% less than the global best solution for the light load and heavy load cases, respectively. When comparing the detailed link quality measurements, the same conclusion can be drawn. Our results illustrate the algorithm's capability to deliver speedy and satisfying connectivity to MC users across a wide range of traffic load situations.

VI. CONCLUSIONS AND FUTURE WORK

In this paper, we presented a data collection system, signaling procedures and machine learning applications for a mission-critical use case, as well as an RL algorithm to autonomously configure and pilot a UAV-BS in order to offer users temporary wireless access. Two novel strategies,

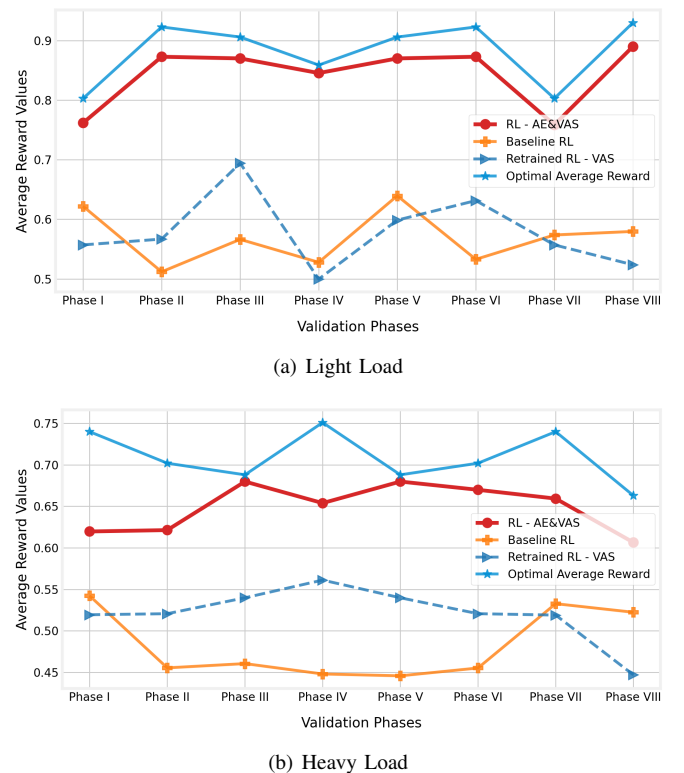


Fig. 9: Average Reward Value in each validation phase

TABLE III: Comparison of the average six link quality metrics with two baseline learning approaches in validation phases

Light Load	DL 50 th Throughput (mbps)	DL 5 th Throughput (mbps)	DL Drop Rate	UL 50 th Throughput (mbps)	UL 5 th Throughput (mbps)	UL Drop Rate	Reward
Optimal State	120.01	21.80	0.52%	8.0	2.11	1.07%	0.881
RL - AE&VAS	103.30	21.08	0%	7.53	2.50	0.03%	0.842
Retrained RL - VAS	99.11	18.33	0.42%	7.06	1.67	1.13%	0.572
Baseline RL	94.28	16.13	1.20%	6.64	1.27	2.15%	0.567
Heavy Load	DL 50 th Throughput (mbps)	DL 5 th Throughput (mbps)	DL Drop Rate	UL 50 th Throughput (mbps)	UL 5 th Throughput (mbps)	UL Drop Rate	Reward
Optimal State	63.98	4.35	17.37%	5.21	0.99	3.77%	0.709
RL - AE&VAS	73.01	6.22	22.59%	5.12	0.78	5.4%	0.648
Retrained RL - VAS	59.76	4.75	20.76%	4.87	0.45	5.12%	0.521
Baseline RL	52.60	3.93	20.60%	4.68	0.36	5.13%	0.483

i.e., adaptive exploration and value-based action selection, are developed to help the proposed RL algorithms work efficiently in a dynamic real-world context, incorporating MC user movements. We show that the proposed RL algorithm can monitor the MC service performance and quickly respond to environmental changes via self-adapting exploration probability. In addition, it requires far fewer model training iterations by reusing previous experience and the value-based action selection strategy. Therefore, the proposed method can well serve the MC users on the ground by autonomously navigating and configuring the UAV-BS despite environmental changes.

In the future, we will consider separating the configuration for access and backhaul antennas of the UAV-BS, as well as modeling drone rotation in the horizontal domain as an addition parameter for the UAV-BS configuration. We also intend to examine other hyper-parameters and reward function combinations based on different service requirements.

REFERENCES

- [1] Y. Zeng, R. Zhang, and T. J. Lim, “Wireless communications with unmanned aerial vehicles: Opportunities and challenges,” *IEEE Communications Magazine*, vol. 54, no. 5, pp. 36–42, 2016.
- [2] J. Li, X. Lin, K. K. Nagalapur, Z. Qi, A. Lahuerta-Lavieja, T. Chapman, S. Agneessens, H. Sahlin, D. Guldbrand, and J. Åkesson, “Towards providing connectivity when and where it counts: An overview of deployable 5G networks,” *arXiv preprint arXiv:2110.05360*, 2021.
- [3] J. Li, K. K. Nagalapur, E. Stare, S. Dwivedi, S. A. Ashraf, P.-E. Eriksson, U. Engström, W. Lee, and T. Lohmar, “5G New Radio for public safety mission critical communications,” *arXiv preprint arXiv:2103.02434*, 2021.
- [4] S. A. R. Naqvi, S. A. Hassan, H. Pervaiz, and Q. Ni, “Drone-aided communication as a key enabler for 5G and resilient public safety networks,” *IEEE Communications Magazine*, vol. 56, no. 1, pp. 36–42, 2018.
- [5] K. P. Morison and J. Calahorrano. (2020) FirstNet Case Study: How FirstNet Deployables are Supporting Public Safety. [Online]. Available: <https://www.policeforum.org/assets/FirstNetDeployables.pdf>
- [6] A. Merwaday, A. Tuncer, A. Kumbhar, and I. Guven, “Improved throughput coverage in natural disasters: Unmanned aerial base stations for public-safety communications,” *IEEE Vehicular Technology Magazine*, vol. 11, no. 4, pp. 53–60, 2016.
- [7] L. Ferranti, L. Bonati, S. D’Oro, and T. Melodia, “SkyCell: A prototyping platform for 5G aerial base stations,” in *2020 IEEE 21st International Symposium on A World of Wireless, Mobile and Multimedia Networks (WoWMoM)*. IEEE, 2020, pp. 329–334.
- [8] H. Wang, H. Zhao, W. Wu, J. Xiong, D. Ma, and J. Wei, “Deployment algorithms of flying base stations: 5G and beyond with UAVs,” *IEEE Internet of Things Journal*, vol. 6, no. 6, pp. 10 009–10 027, 2019.
- [9] E. Kalantari, M. Z. Shakir, H. Yanikomeroglu, and A. Yongacoglu, “Backhaul-aware robust 3D drone placement in 5G+ wireless networks,” in *2017 IEEE international conference on communications workshops (ICC workshops)*. IEEE, 2017, pp. 109–114.
- [10] C. T. Cicek, H. Gultekin, B. Tavli, and H. Yanikomeroglu, “Backhaul-aware optimization of UAV base station location and bandwidth allocation for profit maximization,” *IEEE Access*, vol. 8, pp. 154 573–154 588, 2020.
- [11] N. Tafintsev, D. Moltchanov, M. Gerasimenko, M. Gapeyenko, J. Zhu, S.-p. Yeh, N. Himayat, S. Andreev, Y. Koucheryavy, and M. Valkama, “Aerial access and backhaul in mmWave B5G systems: Performance dynamics and optimization,” *IEEE Communications Magazine*, vol. 58, no. 2, pp. 93–99, 2020.
- [12] S. A. Al-Ahmed, M. Z. Shakir, and S. A. R. Zaidi, “Optimal 3D UAV base station placement by considering autonomous coverage hole detection, wireless backhaul and user demand,” *Journal of Communications and Networks*, vol. 22, no. 6, pp. 467–475, 2020.
- [13] C. Madapatha, B. Makki, C. Fang, O. Teyeb, E. Dahlman, M.-S. Alouini, and T. Svensson, “On integrated access and backhaul networks: Current status and potentials,” *IEEE Open Journal of the Communications Society*, vol. 1, pp. 1374–1389, 2020.
- [14] A. Fouda, A. S. Ibrahim, I. Güvenç, and M. Ghosh, “Interference management in UAV-assisted integrated access and backhaul cellular networks,” *IEEE Access*, vol. 7, pp. 104 553–104 566, 2019.
- [15] M.-A. Lahmeri, M. A. Kishk, and M.-S. Alouini, “Artificial intelligence for UAV-enabled wireless networks: A survey,” *IEEE Open Journal of the Communications Society*, vol. 2, pp. 1015–1040, 2021.
- [16] A. Ly and Y.-D. Yao, “A review of deep learning in 5G research: Channel coding, massive MIMO, multiple access, resource allocation, and network security,” *IEEE Open Journal of the Communications Society*, vol. 2, pp. 396–408, 2021.
- [17] C. H. Liu, Z. Chen, J. Tang, J. Xu, and C. Piao, “Energy-efficient UAV control for effective and fair communication coverage: A deep reinforcement learning approach,” *IEEE Journal on Selected Areas in Communications*, vol. 36, no. 9, pp. 2059–2070, 2018.
- [18] C. Madapatha, B. Makki, A. Muhammad, E. Dahlman, M.-S. Alouini, and T. Svensson, “On topology optimization and routing in integrated access and backhaul networks: A genetic algorithm-based approach,” *IEEE Open Journal of the Communications Society*, vol. 2, pp. 2273–2291, 2021.
- [19] F. Tang, Y. Zhou, and N. Kato, “Deep reinforcement learning for dynamic uplink/downlink resource allocation in high mobility 5G HetNet,” *IEEE Journal on Selected Areas in Communications*, vol. 38, no. 12, pp. 2773–2782, 2020.
- [20] H. Yang, J. Zhao, Z. Xiong, K.-Y. Lam, S. Sun, and L. Xiao, “Privacy-preserving federated learning for UAV-enabled networks: Learning-based joint scheduling and resource management,” *IEEE Journal on Selected Areas in Communications*, vol. 39, no. 10, pp. 3144–3159, 2021.
- [21] C. Zhou, W. Wu, H. He, P. Yang, F. Lyu, N. Cheng, and X. Shen, “Deep reinforcement learning for delay-oriented IoT task scheduling in sagin,” *IEEE Transactions on Wireless Communications*, vol. 20, no. 2, pp. 911–925, 2021.

- [22] S. Tan, C. Dun, F. Jin, and K. Xu, "UAV control in smart city based on space-air-ground integrated network," in *2021 International Conference on Internet, Education and Information Technology (IEIT)*, 2021, pp. 324–328.
- [23] L. Zhang, A. Celik, S. Dang, and B. Shihada, "Energy-efficient trajectory optimization for UAV-assisted IoT networks," *IEEE Transactions on Mobile Computing*, pp. 1–1, 2021.
- [24] S. Yin, S. Zhao, Y. Zhao, and F. R. Yu, "Intelligent trajectory design in UAV-aided communications with reinforcement learning," *IEEE Transactions on Vehicular Technology*, vol. 68, no. 8, pp. 8227–8231, 2019.
- [25] S. Yin and F. R. Yu, "Resource allocation and trajectory design in UAV-aided cellular networks based on multi-agent reinforcement learning," *IEEE Internet of Things Journal*, pp. 1–1, 2021.
- [26] H. Wu, F. Lyu, C. Zhou, J. Chen, L. Wang, and X. Shen, "Optimal UAV caching and trajectory in aerial-assisted vehicular networks: A learning-based approach," *IEEE Journal on Selected Areas in Communications*, vol. 38, no. 12, pp. 2783–2797, 2020.
- [27] C. Wang, J. Wang, Y. Shen, and X. Zhang, "Autonomous navigation of UAVs in large-scale complex environments: A deep reinforcement learning approach," *IEEE Transactions on Vehicular Technology*, vol. 68, no. 3, pp. 2124–2136, 2019.
- [28] C. Wang, J. Wang, J. Wang, and X. Zhang, "Deep-reinforcement-learning-based autonomous UAV navigation with sparse rewards," *IEEE Internet of Things Journal*, vol. 7, no. 7, pp. 6180–6190, 2020.
- [29] H. Huang, Y. Yang, H. Wang, Z. Ding, H. Sari, and F. Adachi, "Deep reinforcement learning for UAV navigation through massive MIMO technique," *IEEE Transactions on Vehicular Technology*, vol. 69, no. 1, pp. 1117–1121, 2020.
- [30] Y. Zeng, X. Xu, S. Jin, and R. Zhang, "Simultaneous navigation and radio mapping for cellular-connected UAV with deep reinforcement learning," *IEEE Transactions on Wireless Communications*, vol. 20, no. 7, pp. 4205–4220, 2021.
- [31] Y. Zeng and R. Zhang, "Energy-efficient UAV communication with trajectory optimization," *IEEE Transactions on Wireless Communications*, vol. 16, no. 6, pp. 3747–3760, 2017.
- [32] S. Ahmed, M. Z. Chowdhury, and Y. M. Jang, "Energy-efficient UAV relaying communications to serve ground nodes," *IEEE Communications Letters*, vol. 24, no. 4, pp. 849–852, 2020.
- [33] C. Zhao, J. Liu, M. Sheng, W. Teng, Y. Zheng, and J. Li, "Multi-UAV trajectory planning for energy-efficient content coverage: A decentralized learning-based approach," *IEEE Journal on Selected Areas in Communications*, vol. 39, no. 10, pp. 3193–3207, 2021.
- [34] B. Zhu, E. Bedeer, H. H. Nguyen, R. Barton, and J. Henry, "UAV trajectory planning in wireless sensor networks for energy consumption minimization by deep reinforcement learning," *IEEE Transactions on Vehicular Technology*, vol. 70, no. 9, pp. 9540–9554, 2021.
- [35] H. Zhang, J. Li, Z. Qi, X. Lin, A. Aronsson, J. Bosch, and H. H. Olsson, "Autonomous navigation and configuration of integrated access backhauling for UAV base station using reinforcement learning," *arXiv preprint arXiv:2112.07313*, 2021.
- [36] 3GPP, "Study on channel model for frequencies from 0.5 to 100 GHz," 3rd Generation Partnership Project (3GPP), Technical Report (TR) 38.901, 1 2020, version 16.1.0. [Online]. Available: https://www.3gpp.org/ftp/Specs/archive/38_series/38.901/38901-g10.zip
- [37] 3GPP, "Study on enhancement for data collection for NR and ENDC," 3rd Generation Partnership Project (3GPP), Technical Report (TR) 37.817, 11 2021, version 0.3.0. [Online]. Available: https://www.3gpp.org/ftp/Specs/archive/37_series/37.817/37817-100.zip
- [38] V. Mnih, K. Kavukcuoglu, D. Silver, A. Graves, I. Antonoglou, D. Wierstra, and M. Riedmiller, "Playing Atari with deep reinforcement learning," *arXiv preprint arXiv:1312.5602*, 2013.
- [39] V. Mnih, K. Kavukcuoglu, D. Silver, A. A. Rusu, J. Veness, M. G. Bellemare, A. Graves, M. Riedmiller, A. K. Fidjeland, G. Ostrovski *et al.*, "Human-level control through deep reinforcement learning," *nature*, vol. 518, no. 7540, pp. 529–533, 2015.
- [40] C. J. C. H. Watkins, "Learning from delayed rewards," 1989.